Performance Evaluation and Interpretation of Unfiltered Feher-Patented Quadrature-Phase-Shift Keying (FQPSK)

M. K. Simon[1] and T.-Y. Yan[1]

A new interpretation of unfiltered Feher-patented quadrature-phase-shift keying (FQPSK) is presented that readily identifies a means for spectral enhancement of the transmitted waveform as well as an improved method of reception. The key to these successes is the replacement of the half-symbol-by-half-symbol mapping originally used to describe FQPSK by a symbol-by-symbol mapping operation combined with memory. The advantages of such an interpretation are twofold. In particular, the original FQPSK scheme can be modified such that the potential of a waveform slope discontinuity at the boundary between half symbols is avoided without sacrificing the "constant" envelope property of the transmitted waveform, and, furthermore, a memory receiver can be employed to improve error-probability performance relative to previously proposed symbol-by-symbol detection methods. The analysis presented in this article does not include other versions of FQPSK such as FQPSK-B, which currently is being considered for military application.

I. Introduction

JPL has been conducting evaluations of efficient modulation technologies for space agencies under the auspices of the Consultative Committee for Space Data Systems (CCSDS) subpanel 1E, RF and Modulation. One of the technologies pursued is the proprietary Feher-patented quadrature-phase-shift keying (FQPSK) modulation format provided to JPL under the Technology Cooperation Agreement between JPL and Digcom Inc. In its generic form, FQPSK as patented [1] and reported in the recent literature [2,3] is *conceptually* the same as the cross-correlated phase-shift-keying (XPSK) modulation technique introduced in 1983 by Kato and Feher [4].[2] This technique was in turn a modification of the previously introduced (by Feher et al. [6]) interference- and jitter-free QPSK (IJF-QPSK) with the express purpose of reducing the 3-dB envelope fluctuation characteristic of IJF-QPSK to 0 dB, thus making it appear constant envelope,[3] which is beneficial in nonlinear radio systems. (It is further noted that, using a constant waveshape for the even pulse and a sinusoidal waveshape for the odd pulse, IJF-QPSK becomes

[1] Communications Systems and Research Section.

[2] Other versions of FQPSK referred to as FQPSK-B [5] include proprietary designed filtering for additional spectrum containment. Such filtering is not germane to our discussions in this article and will not be considered.

[3] The reduction of the envelope from 3 dB to 0 dB occurs only at the uniform sampling instants on the in-phase (I) and quadrature-phase (Q) channels. It is for this reason that XPSK is referred to as being "pseudo"—or "quasi"—constant envelope, i.e., its envelope has a small amount of fluctuation between the uniform sampling instants.

identical to the staggered quadrature overlapped raised-cosine (SQORC) scheme introduced by Austin and Chang [7]). The means by which Kato and Feher achieved their 3-dB envelope reduction was the introduction of an intentional but controlled amount of cross-correlation between the in-phase (I) and quadrature-phase (Q) channels. This cross-correlation operation was applied to the IJF-QPSK (SQORC) baseband signal prior to its modulation onto the I and Q carriers (see Fig. 1). Specifically, this operation was described by mapping *in each half symbol* the 16 possible combinations of I- and Q-channel waveforms present in the SQORC signal into a new[4] set of 16 waveform combinations chosen in such a way that the cross-correlator output is time continuous and has unit (normalized) envelope[5] at all I and Q uniform sampling instants. By virtue of the fact that the cross-correlation mapping is based on a half-symbol characterization of the SQORC signal, there is no guarantee that the *slope* of the cross-correlator output waveform is continuous at the half-symbol transition points. In fact, we shall show that for a random data input sequence such a discontinuity in slope occurs one quarter of the time.

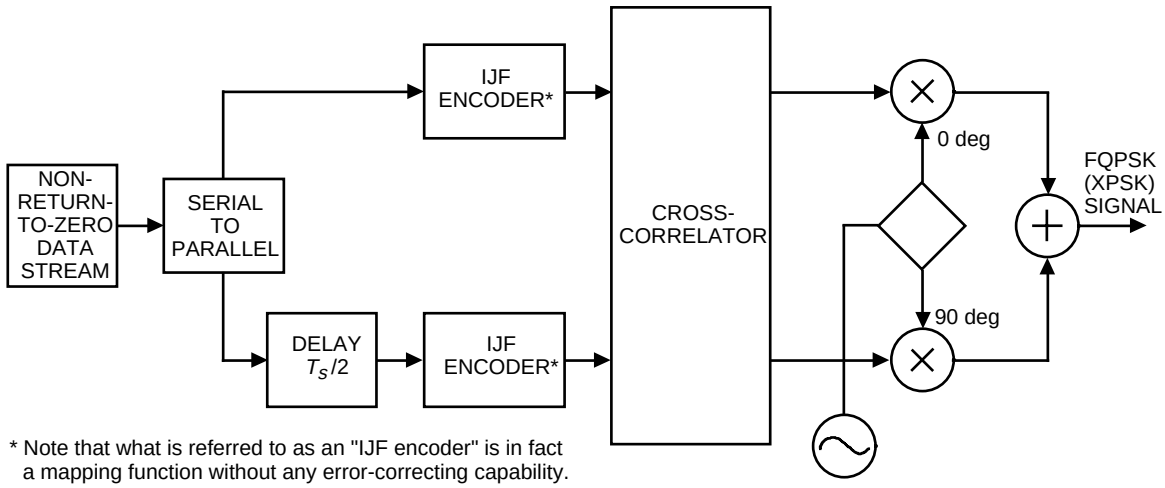

Fig. 1. The conceptual block diagram of FQPSK (XPSK).

It is well-known that the rate at which the side lobes of a modulation's power spectral density (PSD) roll off with frequency is related to the smoothness of the underlying waveforms that generate it. That is, the more derivatives of a waveform that are continuous, the faster its Fourier transform decays with frequency. Thus, since the first derivative of the FQPSK waveform is discontinuous (at half-symbol transition instants) on the average of one-quarter of the time, one can anticipate that an improvement in PSD roll-off could be had if the FQPSK cross-correlation mapping could be modified so that the first derivative is always continuous. By restructuring the cross-correlation mapping into a symbol-by-symbol representation, the slope discontinuity referred to above will be placed in evidence and will be particularly helpful in suggesting a means to eliminate it. This representation also has the advantage that it can be described directly in terms of the data transitions on the I and Q channels and, thus, the combination of IJF encoder and cross-correlator can be replaced simply by a single modified cross-correlator. The replacement of the conventional FQPSK cross-correlator by this modified cross-correlator that eliminates the slope discontinuity leads to what we shall refer to as enchanced FQPSK. We shall show that not only does enhanced FQPSK have a better PSD (in the sense of reduced out-of-band energy) than conventional FQPSK has but, from a modulation symmetry standpoint, it is a more logical choice.

---

[4] Of the 16 possible cross-correlator output combinations, only 12 of them are in fact new, i.e., for 4 of the input I and Q combinations, the cross-correlator outputs the identical combination.

[5] Actually, in the operation's generic form, Kato and Feher allow (through the introduction of a transition parameter, $k = 1 - A$) for a controlled amount of envelope fluctuation. For quasi-constant envelope, one should choose $A = 1/\sqrt{2}$.

A further and more important advantage of the reformulation as a symbol-by-symbol mapping is the ability to design a receiver of FQPSK or enhanced FQPSK (EFQPSK) that specifically exploits the correlation introduced into the modulation scheme to significantly improve power efficiency or, equivalently, error-probability performance. Such a receiver, which takes a form analogous to those used for trellis-coded modulations, will be shown to yield significant performance improvement over receivers that employ symbol-by-symbol detection, thus ignoring the inherent memory of the modulation.

II. Review of IJF-QPSK and SQORC

The IJF-QPSK scheme (alternatively called FQPSK-1) is based on defining waveforms $s_o(t)$ and $s_e(t)$, which are respectively odd and even functions of time over the symbol interval $-T_s/2 \leq t \leq T_s/2$, and then using these and their negatives, $-s_o(t)$ and $-s_e(t)$, as a 4-ary signal set for transmission in accordance with the values of successive pairs of data symbols in each of the I and Q arms. Specifically, if d_{In} denotes the I-channel data symbols in the interval $(n - [1/2])\,T_s \leq t \leq (n + [1/2])\,T_s$, then the transmitted waveform $x_I\,(t)$ in this same interval would be determined as follows:

$$\left.\begin{array}{ll} x_I(t) = s_e\,(t - nT_s) \triangleq s_0\,(t - nT_s) & \textit{if } d_{I,n-1} = 1, d_{I,n} = 1 \\ x_I\,(t) = -\,s_e\,(t - nT_s) \triangleq s_1\,(t - nT_s) & \textit{if } d_{I,n-1} = -1, d_{I,n} = -1 \\ x_I\,(t) = s_0\,(t - nT_s) \triangleq s_2\,(t - nT_s) & \textit{if } d_{I,n-1} = -1, d_{I,n} = 1 \\ x_I\,(t) = -\,s_o\,(t - nT_s) \triangleq s_3\,(t - nT_s) & \textit{if } d_{I,n-1} = 1, d_{I,n} = -1 \end{array}\right\} \tag{1}$$

The Q-channel waveform, $x_Q\,(t)$, would be generated by the same mapping as in Eq. (1), using instead the Q-channel data symbols, $\{d_{Qn}\}$, and then delaying the resulting waveform by one-half of a symbol. If the odd and even waveforms $s_o(t)$ and $s_e(t)$ are defined by

$$\left.\begin{array}{ll} s_e\,(t) = 1, & -\dfrac{T_s}{2} \leq t \leq \dfrac{T_s}{2} \\ s_o\,(t) = \sin\dfrac{\pi t}{T_s}, & -\dfrac{T_s}{2} \leq t \leq \dfrac{T_s}{2} \end{array}\right\} \tag{2}$$

then typical waveforms for the I and Q IJF encoder outputs are as illustrated in Fig. 2.

A modulation identical to $x_I\,(t)$ [and likewise for $x_Q\,(t)$] generated from the combination of Eqs. (1) and (2) can be obtained directly from the binary data sequence $\{d_{In}\}$ itself without the need for defining a 4-ary mapping based on the transition properties of the sequence. In particular, if we define the two-symbol-wide raised-cosine pulse shape

$$p\,(t) = \sin^2\left(\frac{\pi\left(t + \dfrac{T_s}{2}\right)}{2T_s}\right), \quad -\frac{T_s}{2} \leq t \leq \frac{3T_s}{2} \tag{3}$$

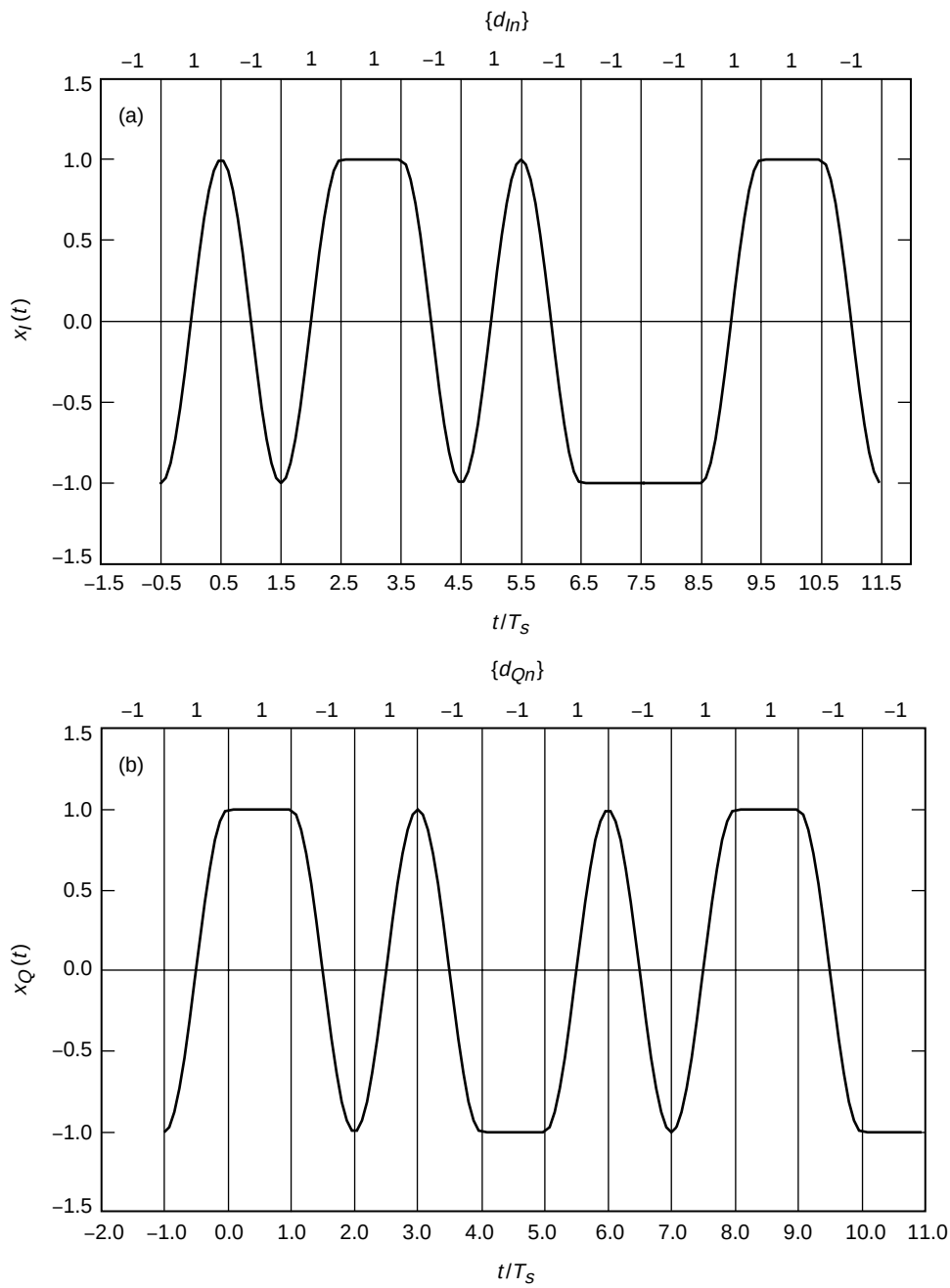

Fig. 2. IJF encoder output: (a) in-phase and (b) quadrature-phase.

then the I modulation

$$x_I(t) \sum_{n=-\infty}^{\infty} d_{In} p(t - nT_s) \tag{4}$$

will be identical to that generated by the above IJF scheme. Similarly,

$$x_Q(t) = \sum_{n=-\infty}^{\infty} d_{Qn} p\left(t - \left(n + \frac{1}{2}\right) T_s\right) \tag{5}$$

also would be identical to that generated by the above IJF scheme. A quadrature modulation scheme formed from $x_I(t)$ of Eq. (4) and $x_Q(t)$ of Eq. (5) is precisely what Austin and Chang [7] referred to as SQORC modulation, namely, independent I and Q modulations with overlapping raised-cosine pulses on each channel. The resulting carrier modulated waveform is described by

$$x(t) = x_I(t) \cos \omega_c t + x_Q(t) \sin \omega_c t \tag{6}$$

III. A Symbol-by-Symbol Cross-Correlator Mapping for FQPSK

Before revealing the modification of FQPSK that results in a transmitted signal having a continuous first derivative, we first recast the original characterization of FQPSK in terms of a cross-correlation operation performed on the pair of IJF encoder outputs every half-symbol interval into a mapping performed directly on the input I and Q data sequences every full-symbol interval. To do this, we define 16 waveforms, $s_i(t)\,;\ i = 0, 1, 2, \cdots, 15$, over the interval $-T_s/2 \le t \le T_s/2$, which collectively form a transmitted signaling set for the I and Q channels. The particular I and Q waveforms chosen for any particular T_s-s signaling interval on each channel depends on the most recent data transition on that channel as well as the two most recent successive transitions on the other channel. The specifics are as follows. Define (see Fig. 3)

$$\left.\begin{aligned}
&s_0(t) = A, \quad -\frac{T_s}{2} \le t \le \frac{T_s}{2}, \quad s_8(t) = -s_0(t) \\
&s_1(t) = \begin{cases} A, & -\frac{T_s}{2} \le t \le 0 \\ 1 - (1-A)\cos^2 \frac{\pi t}{T_s}, & 0 \le t \le \frac{T_s}{2} \end{cases} \quad s_9(t) = -s_1(t) \\
&s_2(t) = \begin{cases} 1 - (1-A)\cos^2 \frac{\pi t}{T_s}, & -\frac{T_s}{2} \le t \le 0 \\ A, & 0 \le t \le \frac{T_s}{2} \end{cases} \quad s_{10}(t) = -s_2(t) \\
&s_3(t) = 1 - (1-A)\cos^2 \frac{\pi t}{T_s}, \quad -\frac{T_s}{2} \le t \le \frac{T_s}{2}, \quad s_{11}(t) = -s_3(t)
\end{aligned}\right\} \tag{7a}$$

and

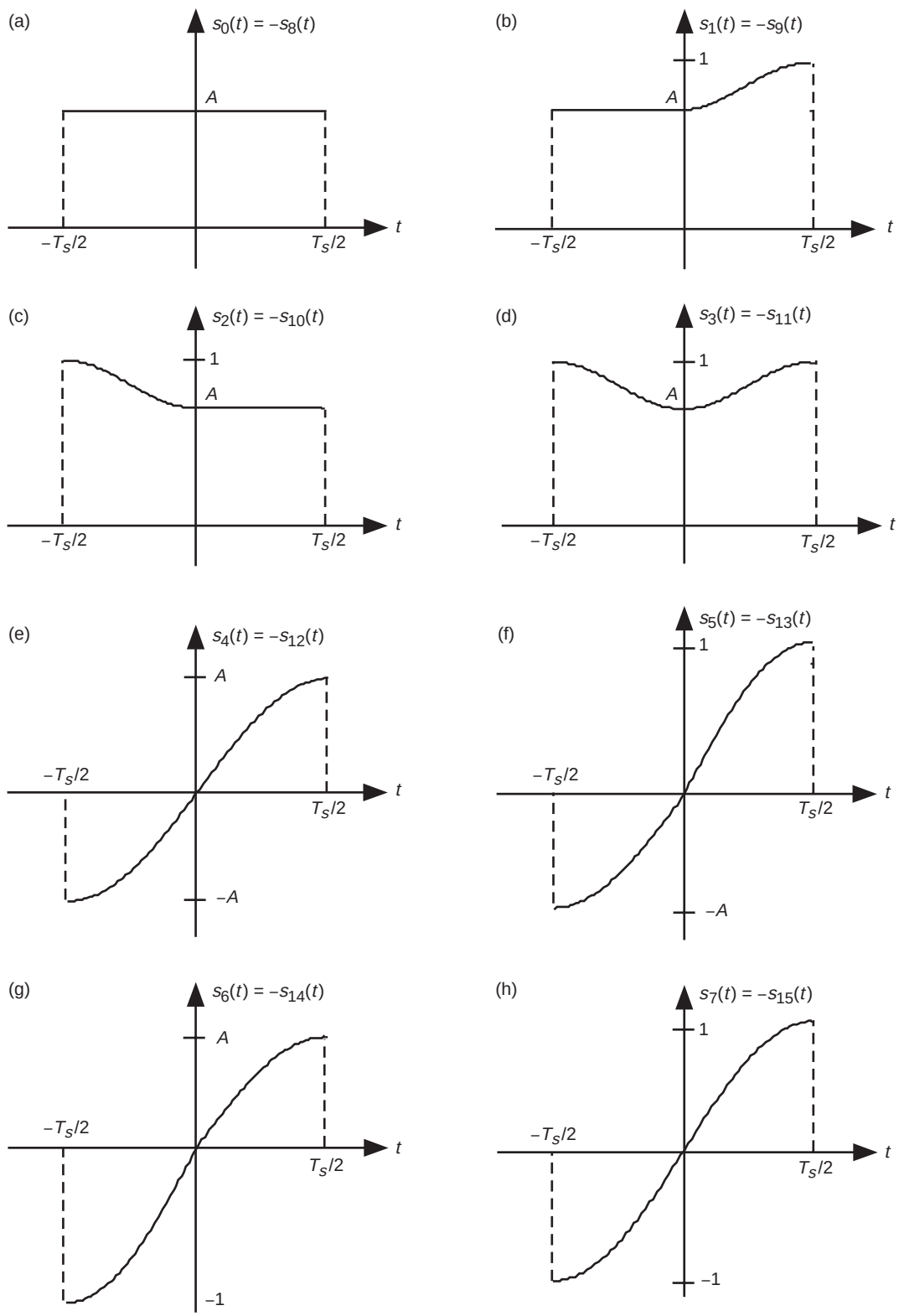

Fig. 3. FQPSK full-symbol waveforms: (a) $s_0(t) = -s_8(t)$ vs t, (b) $s_1(t) = -s_9(t)$ vs t, (c) $s_2(t) = -s_{10}(t)$ vs t, (d) $s_3(t) = -s_{11}(t)$ vs t, (e) $s_4(t) = -s_{12}(t)$ vs t, (f) $s_5(t) = -s_{13}(t)$ vs t, (g) $s_6(t) = -s_{14}(t)$ vs t, and (h) $s_7(t) = -s_{15}(t)$ vs t.

$$
\left.
\begin{array}{ll}
s_4(t) = A\sin\dfrac{\pi t}{T_s}, \quad -\dfrac{T_s}{2} \le t \le \dfrac{T_s}{2}, & s_{12}(t) = -s_4(t) \\[2ex]
s_5(t) = \begin{cases} A\sin\dfrac{\pi t}{T_s}, & -\dfrac{T_s}{2} \le t \le 0 \\[2ex] \sin\dfrac{\pi t}{T_s}, & 0 \le t \le \dfrac{T_s}{2} \end{cases} & s_{13}(t) = -s_5(t) \\[2ex]
s_6(t) = \begin{cases} \sin\dfrac{\pi t}{T_s}, & -\dfrac{T_s}{2} \le t \le 0 \\[2ex] A\sin\dfrac{\pi t}{T_s}, & 0 \le t \le \dfrac{T_s}{2} \end{cases} & s_{14}(t) = -s_6(t) \\[2ex]
s_7(t) = \sin\dfrac{\pi t}{T_s}, \quad -\dfrac{T_s}{2} \le t \le \dfrac{T_s}{2}, & s_{15}(t) = -s_7(t)
\end{array}
\right\} \tag{7b}
$$

Note that for any value of A other then unity, $s_6(t)$ and $s_7(t)$ as well as their negatives, $s_{13}(t)$ and $s_{14}(t)$, will have a discontinuous slope at their midpoints (i.e., at $t = 0$), whereas the remaining 12 waveforms all have a continuous slope throughout their defining intervals. Also, all 16 waveforms have zero slope at their end points and, thus, concatenation of any pair of these will not result in a slope discontinuity.

Next, define the following mapping function for the baseband I-channel transmitted waveform $y_I(t) = s_I(t)$ in the nth signaling interval $(n - [1/2])T_s \le t \le (n + [1/2])T_s$ in terms of the transition properties of the I and Q data symbol sequences $\{d_{In}\}$ and $\{d_{Qn}\}$, respectively.

(1) If $d_{I,n-1} = 1, d_{I,n} = 1$ (no transition on the I sequence, both data bits positive), then

- (a) $y_I(t) = s_0(t - nT_s)$ if $d_{Q,n-2}, d_{Q,n-1}$ results in no transition and $d_{Q,n-1}, d_{Q,n}$ results in no transition.
- (b) $y_I(t) = s_1(t - nT_s)$ if $d_{Q,n-2}, d_{Q,n-1}$ results in no transition and $d_{Q,n-1}, d_{Q,n}$ results in a transition (positive or negative).
- (c) $y_I(t) = s_2(t - nT_s)$ if $d_{Q,n-2}, d_{Q,n-1}$ results in a transition (positive or negative) and $d_{Q,n-1}, d_{Q,n}$ results in no transition.
- (d) $y_I(t) = s_3(t - nT_s)$ if $d_{Q,n-2}, d_{Q,n-1}$ results in a transition (positive or negative) and $d_{Q,n-1}, d_{Q,n}$ results in a transition (positive or negative).

(2) If $d_{I,n-1} = -1, d_{I,n} = 1$ (a positive going transition on the I sequence), then

- (a) $y_I(t) = s_4(t - nT_s)$ if $d_{Q,n-2}, d_{Q,n-1}$ results in no transition and $d_{Q,n-1}, d_{Q,n}$ results in no transition.
- (b) $y_I(t) = s_5(t - nT_s)$ if $d_{Q,n-2}, d_{Q,n-1}$ results in no transition and $d_{Q,n-1}, d_{Q,n}$ results in a transition (positive or negative).
- (c) $y_I(t) = s_6(t - nT_s)$ if $d_{Q,n-2}, d_{Q,n-1}$ results in a transition (positive or negative) and $d_{Q,n-1}, d_{Q,n}$ results in no transition.

(d) $y_I(t) = s_7(t - nT_s)$ if $d_{Q,n-2}, d_{Q,n-1}$ results in a transition (positive or negative) and $d_{Q,n-1}, d_{Q,n}$ results in a transition (positive or negative).

(3) If $d_{I,n-1} = -1, d_{I,n} = -1$ (no transition on the I sequence, both data bits negative), then

(a) $y_I(t) = s_8(t - nT_s)$ if $d_{Q,n-2}, d_{Q,n-1}$ results in no transition and $d_{Q,n-1}, d_{Q,n}$ results in no transition.

(b) $y_I(t) = s_9(t - nT_s)$ if $d_{Q,n-2}, d_{Q,n-1}$ results in no transition and $d_{Q,n-1}, d_{Q,n}$ results in a transition (positive or negative).

(c) $y_I(t) = s_{10}(t - nT_s)$ if $d_{Q,n-2}, d_{Q,n-1}$ results in a transition (positive or negative) and $d_{Q,n-1}, d_{Q,n}$ results in no transition.

(d) $y_I(t) = s_{11}(t - nT_s)$ if $d_{Q,n-2}, d_{Q,n-1}$ results in a transition (positive or negative) and $d_{Q,n-1}, d_{Q,n}$ results in a transition (positive or negative).

(4) If $d_{I,n-1} = 1, d_{I,n} = -1$ (a negative going transition on the I sequence), then

(a) $y_I(t) = s_{12}(t - nT_s)$ if $d_{Q,n-2}, d_{Q,n-1}$ results in no transition and $d_{Q,n-1}, d_{Q,n}$ results in no transition.

(b) $y_I(t) = s_{13}(t - nT_s)$ if $d_{Q,n-2}, d_{Q,n-1}$ results in no transition and $d_{Q,n-1}, d_{Q,n}$ results in a transition (positive or negative).

(c) $y_I(t) = s_{14}(t - nT_s)$ if $d_{Q,n-2}, d_{Q,n-1}$ results in a transition (positive or negative) and $d_{Q,n-1}, d_{Q,n}$ results in no transition.

(d) $y_I(t) = s_{15}(t - nT_s)$ if $d_{Q,n-2}, d_{Q,n-1}$ results in a transition (positive or negative) and $d_{Q,n-1}, d_{Q,n}$ results in a transition (positive or negative).

Making use of the signal properties in Eqs. (7a) and (7b), the mapping conditions in (1) through (4) for the I-channel baseband output can be summarized in a concise form described by Table 1. A similar construction for the baseband Q-channel transmitted waveform $y_Q(t) = s_Q(t - T_s/2)$ in the nth signaling interval $nT_s \leq t \leq (n+1)T_s$ in terms of the transition properties of the I and Q data symbol sequences, $\{d_{In}\}$ and $\{d_{Qn}\}$, respectively, can be obtained analogously to (1) through (4) above. The results can once again be summarized in the form of a table, as in Table 2.

Table 1. Mapping for I-channel baseband signal $y_I(t)$ in the interval $(n - [1/2])\,T_S \leq t \leq (n + [1/2])\,T_S$.

$\left\lvert\frac{d_{In}-d_{I,n-1}}{2}\right\rvert$	$\left\lvert\frac{d_{Q,n-1}-d_{Q,n-2}}{2}\right\rvert$	$\left\lvert\frac{d_{Q,n}-d_{Q,n-1}}{2}\right\rvert$	$s_I(t)$
0	0	0	$d_{In}s_0(t-nT_s)$
0	0	1	$d_{In}s_1(t-nT_s)$
0	1	0	$d_{In}s_2(t-nT_s)$
0	1	1	$d_{In}s_3(t-nT_s)$
1	0	0	$d_{In}s_4(t-nT_s)$
1	0	1	$d_{In}s_5(t-nT_s)$
1	1	0	$d_{In}s_6(t-nT_s)$
1	1	1	$d_{In}s_7(t-nT_s)$

Table 2. Mapping for Q-channel baseband signal $y_Q(t)$ in the interval $nT_s \le t \le (n+1)\,T_s$.[a]

$\left\lvert \frac{d_{Qn}-d_{Q,n-1}}{2} \right\rvert$	$\left\lvert \frac{d_{I,n}-d_{I,n-1}}{2} \right\rvert$	$\left\lvert \frac{d_{I,n+1}-d_{I,n}}{2} \right\rvert$	$s_I(t)$
0	0	0	$d_{Qn}s_0(t-nT_s)$
0	0	1	$d_{Qn}s_1(t-nT_s)$
0	1	0	$d_{Qn}s_2(t-nT_s)$
0	1	1	$d_{Qn}s_3(t-nT_s)$
1	0	0	$d_{Qn}s_4(t-nT_s)$
1	0	1	$d_{Qn}s_5(t-nT_s)$
1	1	0	$d_{Qn}s_6(t-nT_s)$
1	1	1	$d_{Qn}s_7(t-nT_s)$

[a] Note that the subscript i of the transmitted signal $s_i\,(t-nT_s)$ or $s_i\,(t-(n+[1/2])\,T_s)$ as appropriate is the binary coded decimal (BCD) equivalent of the three transitions!

Applying the mappings in Tables 1 and 2 to the I and Q data sequences of Fig. 2 produces the identical I and Q baseband transmitted signals to those that would be produced by passing the I and Q IJF encoder outputs of this figure through the cross-correlator (half-symbol mapping) of the FQPSK (XPSK) scheme as described in [4] (see Fig. 4). Thus, we conclude that *for arbitrary I and Q input sequences, FQPSK can alternatively be generated by the symbol-by-symbol mappings of Tables 1 and 2 as applied to these sequences.*

IV. A New and Improved FQPSK

As discussed above, the symbol-by-symbol mapping representation of FQPSK identifies the fact that 4 out of the 16 possible transmitted waveforms, namely, $s_5\,(t)\,, s_6\,(t)\,, s_{13}\,(t)\,,$ and $s_{14}\,(t)$, have a slope discontinuity at their midpoints. Thus, for random I and Q data symbol sequences, the transmitted FQPSK waveform on the average likewise will have a slope discontinuity at one-quarter of the uniform-sampling time instants. To prevent this from occurring, we now redefine these four transmitted signals in a manner analogous to $s_1\,(t)\,, s_2\,(t)\,, s_9\,(t)\,,$ and $s_{10}\,(t)$, namely,

$$\left.\begin{aligned}
s_5\,(t) &= \begin{cases} \sin\dfrac{\pi t}{T_s} + (1-A)\sin^2\dfrac{\pi t}{T_s}, & -\dfrac{T_s}{2} \le t \le 0 \\[2ex] \sin\dfrac{\pi t}{T_s}, & 0 \le t \le \dfrac{T_s}{2} \end{cases} \qquad s_{13}\,(t) = -s_5\,(t) \\[4ex]
s_6\,(t) &= \begin{cases} \sin\dfrac{\pi t}{T_s}, & -\dfrac{T_s}{2} \le t \le 0 \\[2ex] \sin\dfrac{\pi t}{T_s} - (1-A)\sin^2\dfrac{\pi t}{T_s}, & 0 \le t \le \dfrac{T_s}{2} \end{cases} \qquad s_{14}\,(t) = -s_6\,(t)
\end{aligned}\right\} \tag{8}$$

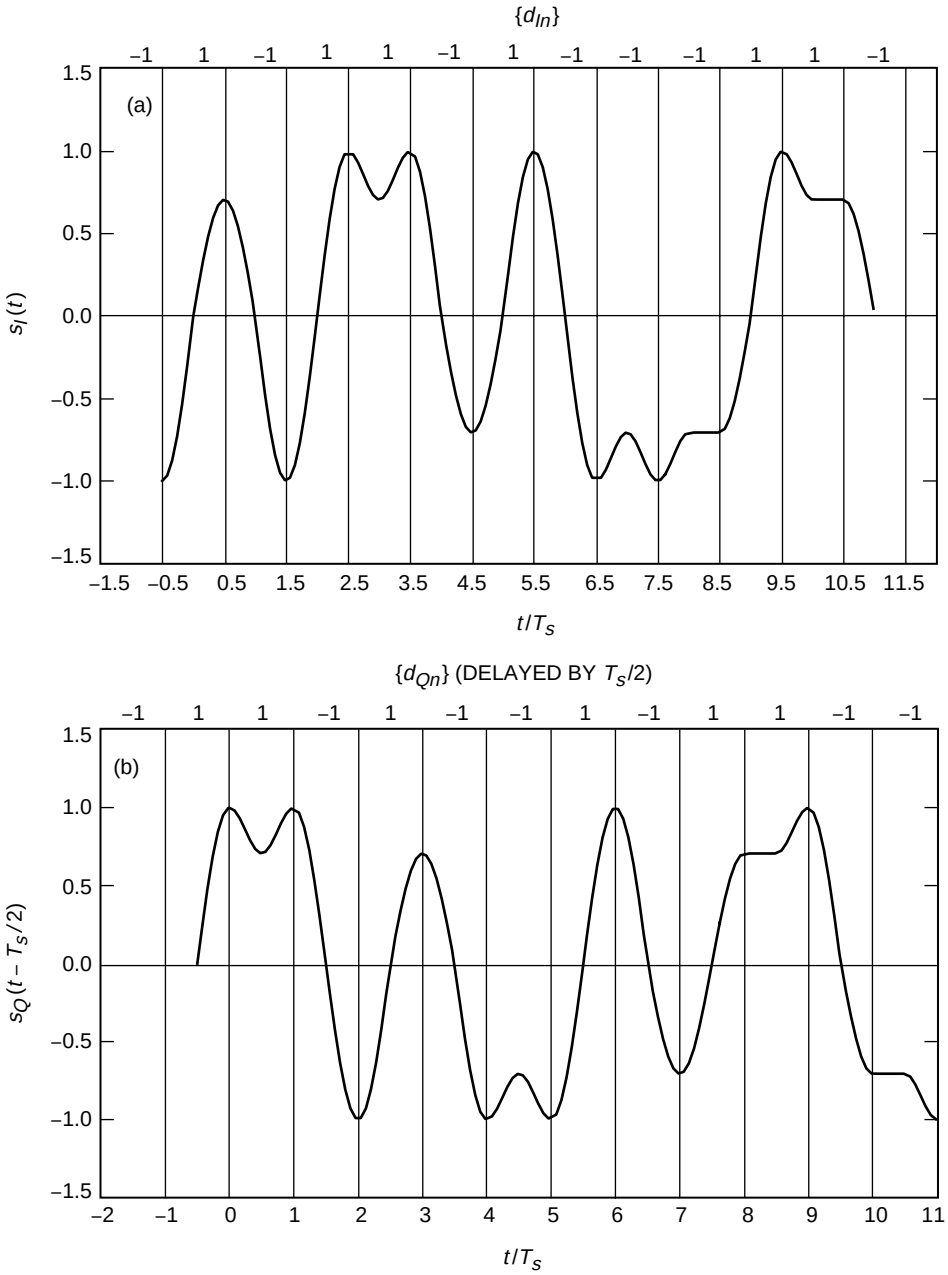

Fig. 4. FQPSK (XPSK) output: (a) in-phase and (b) quadrature-phase.

Note that the signals $s_5(t), s_6(t), s_{13}(t)$, and $s_{14}(t)$, as defined in Eq. (8), do *not* have a slope discontinuity at their midpoints nor for that matter anywhere else in the defining intervals. Also, the zero slopes at their end points have been preserved. Thus, using Eq. (8) in place of the corresponding signals of Eq. (7b) will result in a modified FQPSK signal that has no slope discontinuity anywhere in time *regardless of the value of* A. Figure 5 illustrates a comparison of the signal $s_6(t)$ of Eq. (8) with that of Eq. (7b) for a value of $A = 1/\sqrt{2}$. Figure 6 illustrates the power spectral density of conventional FQPSK and its enhancement, EFQPSK, obtained by using the waveforms of Eq. (8) as replacements for those in Eq. (7b). The significant improvement in spectral roll-off rate is clear from a comparison of the two.

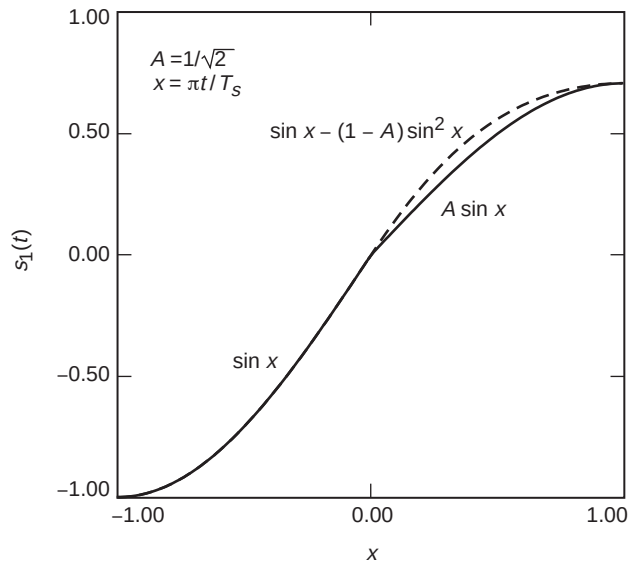

Fig. 5. Original and new FQPSK pulse shapes.

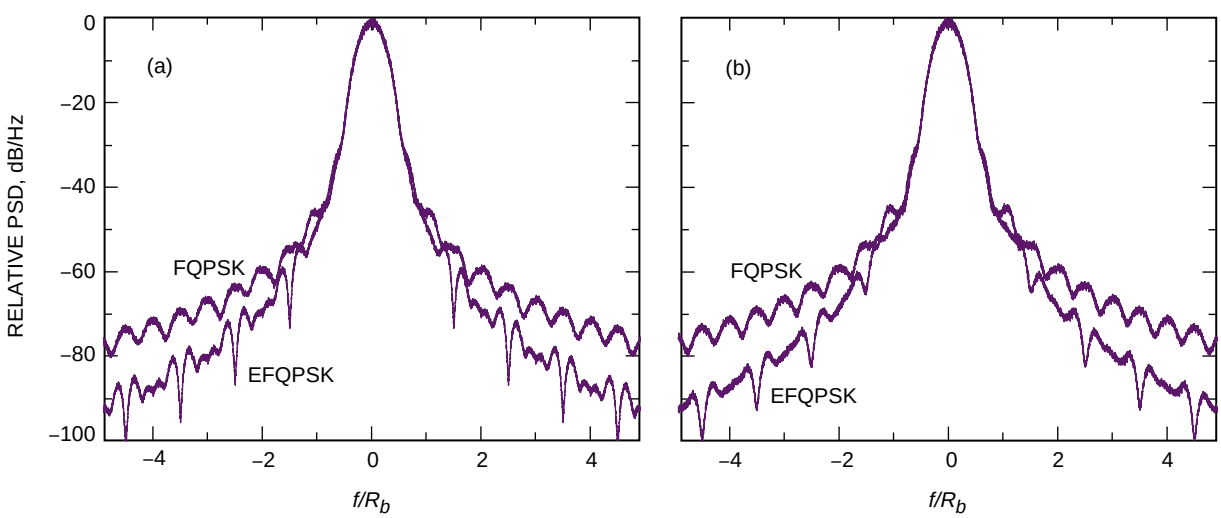

Fig. 6. Power spectra of conventional and enhanced FQPSK: (a) without SSPA and (b) with SSPA.

As it currently stands, the signal set chosen for EFQPSK has a symmetry property for $s_0(t), s_1(t)$, $s_2(t)$, and $s_3(t)$ that is not present for $s_4(t), s_5(t), s_6(t)$, and $s_7(t)$. In particular, $s_1(t)$ and $s_2(t)$ are each composed of one-half of $s_0(t)$ and one-half of $s_3(t)$, i.e., the portion of $s_1(t)$ from $t = -T_s/2$ to $t = 0$ is the same as that of $s_0(t)$, whereas the portion of $s_1(t)$ from $t = 0$ to $t = T_s/2$ is the same as that of $s_3(t)$ and vice versa for $s_2(t)$. To achieve the same symmetry property for $s_4(t) - s_7(t)$, one would have to reassign $s_4(t)$ as

$$s_4(t) = \begin{cases} \sin\dfrac{\pi t}{T_s} + (1-A)\sin^2\dfrac{\pi t}{T_s}, & -\dfrac{T_s}{2} \le t \le 0 \\ \\ \sin\dfrac{\pi t}{T_s} - (1-A)\sin^2\dfrac{\pi t}{T_s}, & 0 \le t \le \dfrac{T_s}{2} \end{cases} \qquad s_{12}(t) = -s_4(t) \tag{9}$$

This minor change, which produces a complete symmetry in the waveform set, has an advantage from the standpoint of hardware implementation and produces a negligible change in spectral properties of the transmitted waveform. Nevertheless, for the remainder of the discussion, we shall ignore this minor change and assume the version of enhanced FQPSK first introduced in this section.

V. Interpretation of FQPSK as a Trellis-Coded Modulation

The I and Q mappings given in Tables 1 and 2 can alternatively be described in terms of the (0,1) representation of the I and Q data symbols and their transitions. Specifically, define

$$\left.\begin{aligned} D_{In} &\triangleq \frac{1-d_{In}}{2} \\ D_{Qn} &\triangleq \frac{1-d_{Qn}}{2} \end{aligned}\right\} \tag{10}$$

which both range over the set (0,1). Then, defining the binary-coded decimal (BCD) representation of the indices i and j by

$$\left.\begin{aligned} i &= I_3 \times 2^3 + I_2 \times 2^2 + I_1 \times 2^1 + I_0 \times 2^0 \\ j &= Q_3 \times 2^3 + Q_2 \times 2^2 + Q_1 \times 2^1 + Q_0 \times 2^0 \end{aligned}\right\} \tag{11}$$

with

$$\left.\begin{aligned} I_0 &= D_{Qn} \oplus D_{Q,n-1}, & Q_0 &= D_{I,n+1} \oplus D_{In} \\ I_1 &= D_{Q,n-1} \oplus D_{Q,n-2}, & Q_1 &= D_{In} \oplus D_{I,n-1} = I_2 \\ I_2 &= D_{In} \oplus D_{I,n-1}, & Q_2 &= D_{Qn} \oplus D_{Q,n-1} = I_0 \\ I_3 &= D_{In}, & Q_3 &= D_{Qn} \end{aligned}\right\} \tag{12}$$

we have $y_I(t) = s_i(t - nT_s)$ and $y_Q(t) = s_j(t - (n + [1/2])T_s)$. That is, in each symbol interval $[(n - [1/2])T_s \le t \le (n + [1/2])T_s$ for $y_I(t)$ and $nT_s \le t \le (n+1)T_s$ for $y_Q(t)]$, the I- and Q-channel baseband signals are each chosen from a set of 16 signals, $s_i(t)$, $i = 0, 1, \cdots, 15$, in accordance with the 4-bit BCD representations of their indices defined by Eq. (11) together with Eq. (12). A graphical illustration of the implementation of this mapping is given in Fig. 7.

Another interpretation of the mapping in Fig. 7 is as a 16-state trellis code with two binary (0,1) inputs, $D_{I,n+1}$ and D_{Qn}, and two waveform outputs, $s_i(t)$ and $s_j(t)$, where the state is defined by the 4-bit sequence $D_{In}, D_{I,n-1}, D_{Q,n-1}, D_{Q,n-2}$. The trellis is illustrated in Fig. 8, and the transition mapping is given in Table 3. In this table, the entries in the column labeled "input" correspond to the values of the two input bits $D_{I,n+1}$ and D_{Qn} that result in the transition, while the entries in the "output" column correspond to the subscripts i and j of the pair of symbol waveforms $s_i(t)$ and $s_j(t)$ that are output.

To compute the performance of this trellis-coded modulation (TCM), we need to determine the minimum Euclidean distance between pairs of error-event paths that leave a given state and first return to

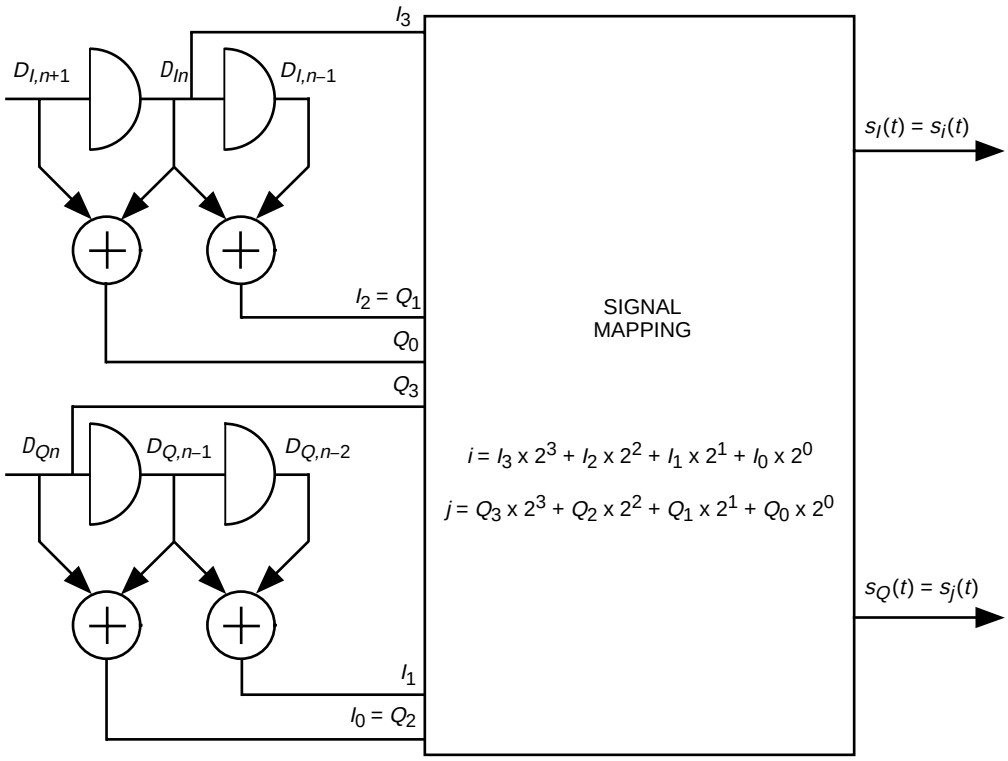

Fig. 7. Alternate implementation of FQPSK baseband signals.

Table 3. Trellis state transitions.

Current state	Input	Output	Next state
0 0 0 0	0 0	0 0	0 0 0 0
0 0 0 0	0 1	1 12	0 0 1 0
0 0 0 0	1 0	0 1	1 0 0 0
0 0 0 0	1 1	1 13	1 0 1 0
0 0 1 0	0 0	3 4	0 0 0 1
0 0 1 0	0 1	2 8	0 0 1 1
0 0 1 0	1 0	3 5	1 0 0 1
0 0 1 0	1 1	2 9	1 0 1 1
1 0 0 0	0 0	12 3	0 1 0 0
1 0 0 0	0 1	13 15	0 1 1 0
1 0 0 0	1 0	12 2	1 1 0 0
1 0 0 0	1 1	13 14	1 1 1 0
1 0 1 0	0 0	15 7	0 1 0 1
1 0 1 0	0 1	14 11	0 1 1 1
1 0 1 0	1 0	15 6	1 1 0 1
1 0 1 0	1 1	14 10	1 1 1 1
0 0 0 1	0 0	2 0	0 0 0 0
0 0 0 1	0 1	3 12	0 0 1 0
0 0 0 1	1 0	2 1	1 0 0 0
0 0 0 1	1 1	3 13	1 0 1 0

Table 3 (contd). Trellis state transitions.

Current state	Input	Output	Next state
0 0 1 1	0 0	1 4	0 0 0 1
0 0 1 1	0 1	0 8	0 0 1 1
0 0 1 1	1 0	1 5	1 0 0 1
0 0 1 1	1 1	0 9	1 0 1 1
1 0 0 1	0 0	14 3	0 1 0 0
1 0 0 1	0 1	15 15	0 1 1 0
1 0 0 1	1 0	14 2	1 1 0 0
1 0 0 1	1 1	15 14	1 1 1 0
1 0 1 1	0 0	13 7	0 1 0 1
1 0 1 1	0 1	12 11	0 1 1 1
1 0 1 1	1 0	13 6	1 1 0 1
1 0 1 1	1 1	12 10	1 1 1 1
0 1 0 0	0 0	4 2	0 0 0 0
0 1 0 0	0 1	5 14	0 0 1 0
0 1 0 0	1 0	4 3	1 0 0 0
0 1 0 0	1 1	5 15	1 0 1 0
0 1 1 0	0 0	7 6	0 0 0 1
0 1 1 0	0 1	6 10	0 0 1 1
0 1 1 0	1 0	7 7	1 0 0 1
0 1 1 0	1 1	6 11	1 0 1 1
1 1 0 0	0 0	8 1	0 1 0 0
1 1 0 0	0 1	9 13	0 1 1 0
1 1 0 0	1 0	8 0	1 1 0 0
1 1 0 0	1 1	9 12	1 1 1 0
1 1 1 0	0 0	11 5	0 1 0 1
1 1 1 0	0 1	10 9	0 1 1 1
1 1 1 0	1 0	11 4	1 1 0 1
1 1 1 0	1 1	10 8	1 1 1 1
0 1 0 1	0 0	6 2	0 0 0 0
0 1 0 1	0 1	7 14	0 0 1 0
0 1 0 1	1 0	6 3	1 0 0 0
0 1 0 1	1 1	7 15	1 0 1 0
0 1 1 1	0 0	5 6	0 0 0 1
0 1 1 1	0 1	4 10	0 0 1 1
0 1 1 1	1 0	5 7	1 0 0 1
0 1 1 1	1 1	4 11	1 0 1 1
1 1 0 1	0 0	10 1	0 1 0 0
1 1 0 1	0 1	11 13	0 1 1 0
1 1 0 1	1 0	10 0	1 1 0 0
1 1 0 1	1 1	11 12	1 1 1 0
1 1 1 1	0 0	9 5	0 1 0 1
1 1 1 1	0 1	8 9	0 1 1 1
1 1 1 1	1 0	9 4	1 1 0 1
1 1 1 1	1 1	8 8	1 1 1 1

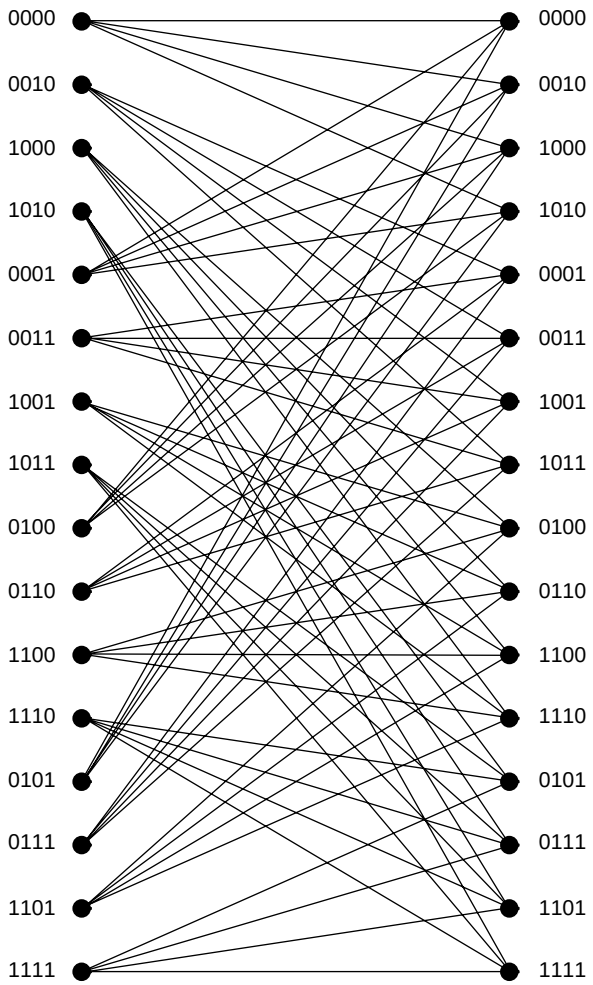

Fig. 8. The 16-state trellis diagram for FQPSK.

that or another state a number of branches later. The smallest-length error event for which there are at least two paths that start in one state and remerge in the same or another state is 3 branches. For each of the 16 starting states, there are exactly 4 such error-event paths that remerge in each of the 16 end states. Figures 9(a) and 9(b) are examples of these error-event paths corresponding to the first two states, respectively, for the case when the start and end states are the same. The remaining length-3 error-event paths for states 9 through 16 are the mirror images of the ones for states 1 through 8 [see, for example, Fig. 9(c), which should be compared with Fig. 9(a)]. Also, the paths for states 9 through 16 will have Euclidean distance properties identical to those for states 1 through 8 since the output symbols along their branches will be the negatives of those along their mirror images. Figures 10(a) and 10(b) are examples of the groups of 4 error-event paths that start in a given state and remerge in another state. A similar mirror-image symmetry exists for these groups of paths and, thus, once again it is sufficient to consider only the first 8 starting states.

It is important to note that the trellis code defined by the mapping in Table 3 is not uniform, e.g., it is not sufficient to consider only the all-zeros path as the transmitted path in computing the minimum Euclidean distance. Rather, one must consider all possible pairs of error-event paths starting from each of the 16 states (8 states is sufficient in view of the above-mentioned distance symmetry properties) and ending in each of the 16 states and determine the pair having the minimum Euclidean distance. The following example illustrates the procedure for the groups of paths that start and end in the same state.

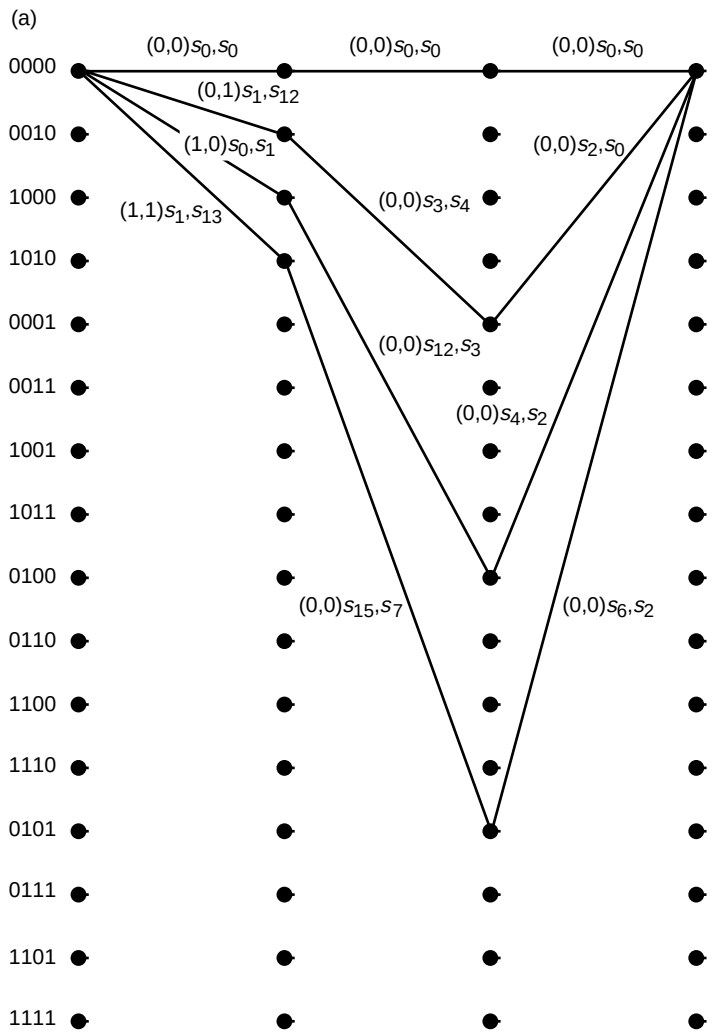

Fig. 9. Paths of length-3 branches starting and ending in (a) state 1, (b) state 2, and (c) state 16.

Upon examination of the squared Euclidean distance between all pairs of paths in the above-mentioned figures, it can be shown that the minimum of this distance, i.e., $d^2_{\min}$, occurs between the first and third paths of Fig. 9(b).[6] Thus, based on the output symbols that occur along this pair of paths, we have

$$d^2_{\min} = \int_{-T_s/2}^{T_s/2} \Big[(s_3(t) - s_3(t))^2 + (s_4(t) - s_5(t))^2 + (s_2(t) - s_{14}(t))^2 + (s_0(t) - s_3(t))^2$$

$$+ (s_1(t) - s_5(t))^2 + (s_{12}(t) - s_{14}(t))^2 \Big] \, dt \tag{13}$$

Evaluation of the squared Euclidean distances between the pairs of waveforms required in Eq. (13) using Eqs. (7a) and (7b) for their definitions results, after much algebra, in

[6] It also occurs between several other pairs of paths starting and ending in the same state.

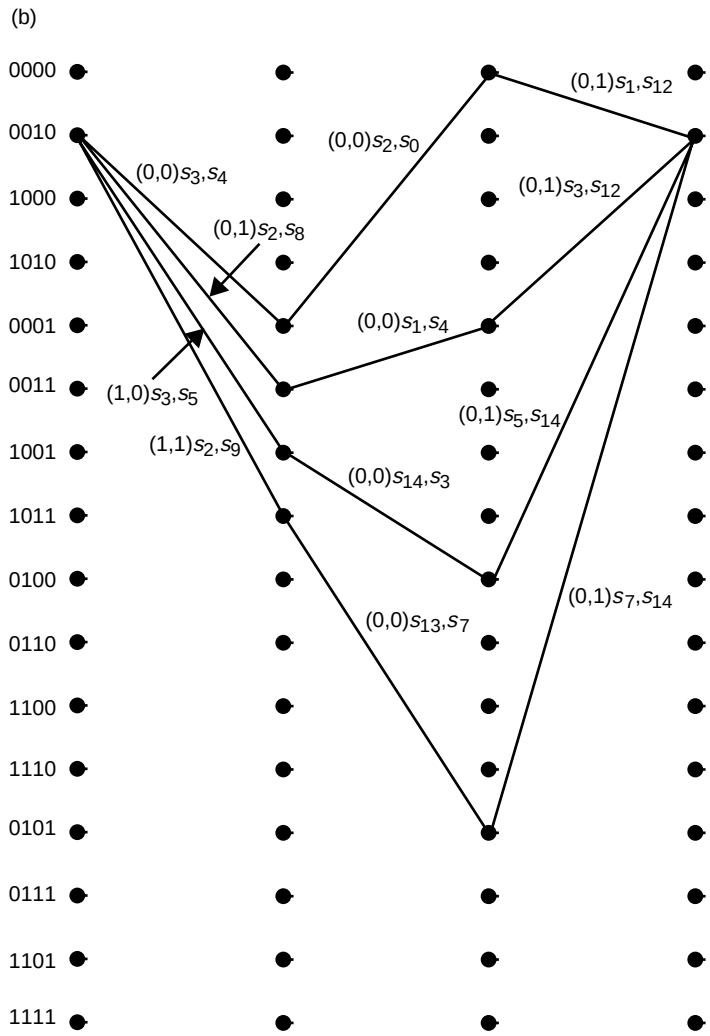

Fig. 9 (contd). Paths of length-3 branches starting and ending in (a) state 1, (b) state 2, and (c) state 16.

$$d_{\min}^2 = \left[\frac{7}{4} - \frac{8}{3\pi} - A\left(\frac{3}{2} + \frac{4}{3\pi}\right) + A^2\left(\frac{11}{4} + \frac{4}{\pi}\right)\right] T_s = 1.552 T_s \tag{14}$$

The average signal $(I + Q)$ energy is obtained from

$$E_{av} = \frac{1}{256}\sum_{i=0}^{15}\sum_{j=0}^{15}\int_{-T_s/2}^{T_s/2}\left[s_i^2(t) + s_j^2(t)\right] dt = 2\left[\frac{1}{16}\sum_{i=0}^{15}\int_{-T_s/2}^{T_s/2} s_i^2(t)\, dt\right] = \frac{1}{4}\sum_{i=0}^{7}\int_{-T_s/2}^{T_s/2} s_i^2(t)\, dt \tag{15}$$

which, again using Eqs. (7a) and (b), evaluates to

$$E_{av} = \left(\frac{7 + 2A + 15A^2}{16}\right) T_s = 0.9946 T_s \tag{16}$$

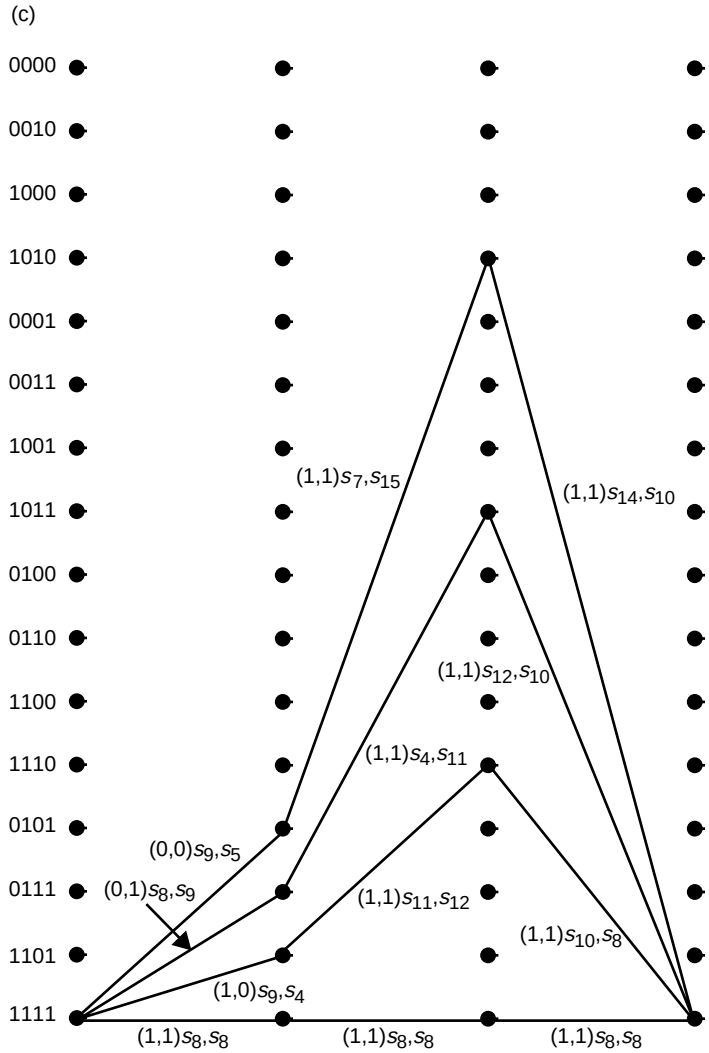

Fig. 9 (contd). Paths of length-3 branches starting and ending in (a) state 1, (b) state 2, and (c) state 16.

Since the average signal (symbol) energy is twice the average energy per bit, $\bar{E}_b$, then the normalized minimum squared Euclidean distance for the paths corresponding to starting and ending in the same state is

$$\frac{d^2_{\min}}{2\bar{E}_b} = \frac{16\left[\frac{7}{4} - \frac{8}{3\pi} - A\left(\frac{3}{2} + \frac{4}{3\pi}\right) + A^2\left(\frac{11}{4} + \frac{4}{\pi}\right)\right]}{(7 + 2A + 15A^2)} = 1.56 \tag{17}$$

Upon examination of all length-3 error-event paths that begin in one state and end in another, e.g., Figs. 10(a) and 10(b), no pair of paths with smaller normalized minimum squared Euclidean distance was found. Furthermore, by exhaustive search, it can be shown that the minimum squared Euclidean distance of Eq. (17) is the smallest over all pairs of paths that start in any state and end in any state regardless of the length of the path. Thus, *the normalized minimum squared Euclidean distance for the FQPSK scheme is given by Eq. (17).*

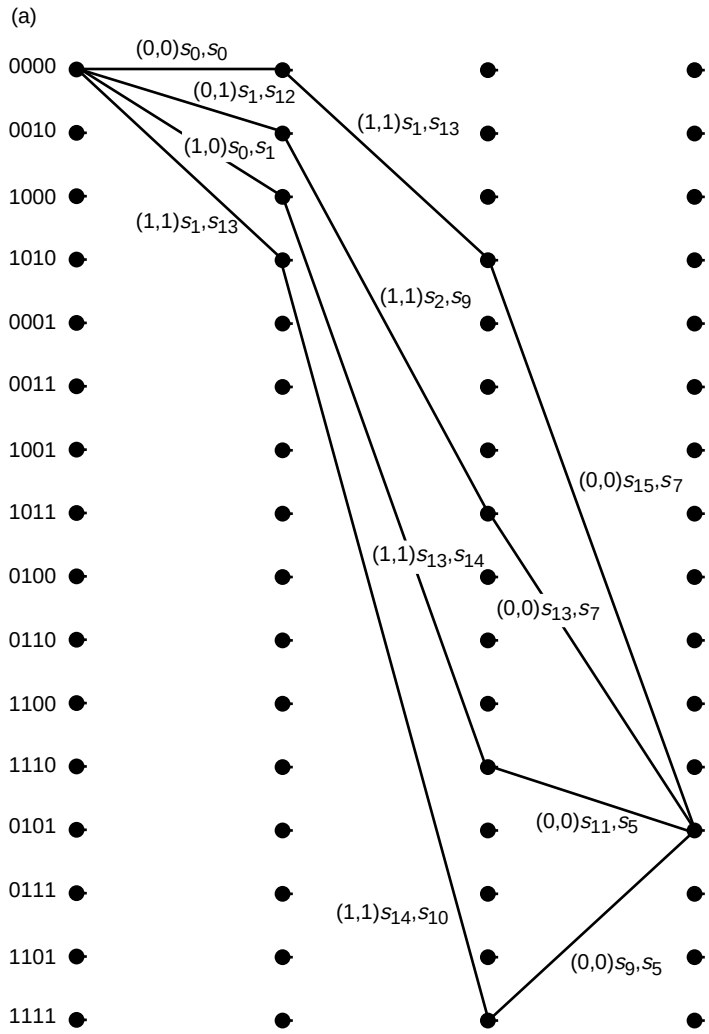

Fig. 10. Paths of length-3 branches starting in state 1 and ending in (a) state 13 and (b) state 2.

For the spectrally enhanced FQPSK using the waveforms of Eq. (8) as replacements for their equivalents in Eq. (7b), the minimum squared Euclidean distance over all length-3 trellis paths occurs, for example, between the first and second paths, starting and ending in state "0000" and is given by [see Fig. 9(a)]

$$d_{\min}^2 = \int_{-T_s/2}^{T_s/2} \Big[\left(s_0(t) - s_1(t)\right)^2 + \left(s_0(t) - s_{12}(t)\right)^2 + \left(s_0(t) - s_3(t)\right)^2 + \left(s_0(t) - s_4(t)\right)^2$$

$$+ \left(s_0(t) - s_2(t)\right)^2 + \left(s_0(t) - s_0(t)\right)^2 \Big] dt \tag{18}$$

Once again, evaluation of the squared Euclidean distances between the pairs of waveforms required in Eq. (18), using Eqs. (7a) and (7b) together now with Eq. (8) for their definitions, results, after much algebra, in

$$d_{\min}^2 = \left[\frac{3 - 6A + 15A^2}{4} \right] T_s = 1.564 T_s \tag{19}$$

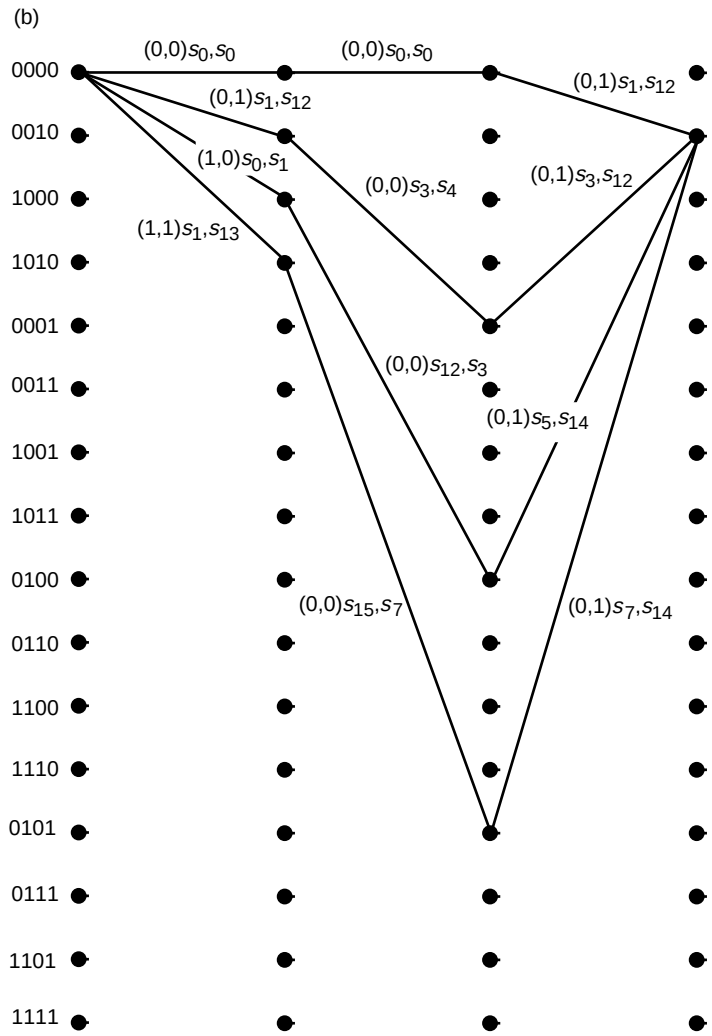

Fig. 10 (contd). Paths of length-3 branches starting in state 1 and ending in (a) state 13 and (b) state 2.

Likewise, the average signal energy is now

$$E_{av} = \left(\frac{\frac{21}{8} - \frac{8}{3\pi} - A\left(\frac{1}{4} - \frac{8}{3\pi}\right) + \frac{29}{8}A^2}{4} \right) T_s = 1.003 T_s \tag{20}$$

Thus, the normalized minimum squared Euclidean distance is

$$\frac{d^2_{\min}}{2\bar{E}_b} = \frac{\left(3 - 6A + 15A^2\right)}{\frac{21}{8} - \frac{8}{3\pi} - A\left(\frac{1}{4} - \frac{8}{3\pi}\right) + \frac{29}{8}A^2} = 1.56 \tag{21}$$

which coincidentally is identical to that for FQPSK. Again there is no other pair of paths starting in any state and ending in any other that produces a smaller normalized minimum squared Euclidean distance.

Thus, we conclude that *the enhancement of FQPSK provided by using the waveforms of Eq. (8) as replacements for their equivalents in Eq. (7b) is significantly beneficial from a spectral standpoint with no penalty in receiver performance.*

In accordance with the foregoing representation of FQPSK as a trellis-coded modulation with 16 states, the optimum receiver (employing a Viterbi algorithm) for FQPSK is illustrated in Fig. 11. Later on, in Section VII, we shall illustrate average bit-error probability (BEP) results obtained from a simulation of this receiver. For the moment, we shall just compare its asymptotic (limit of infinite energy-to-noise ratio) performance with that of the optimum receiver for conventional uncoded offset QPSK (OQPSK). Since for the latter $d^2_{\min}/2\bar{E}_b = 2$, which is the same as that for BPSK [8], then we see that as a trade against the significantly improved power spectrum afforded by FQPSK and its enhanced version relative to that of OQPSK, *an asymptotic loss of only* $10\log(1/1.56) = 1.07$ *dB is experienced.*[7]

VI. Symbol-by-Symbol Detection of FQPSK

In this section, we examine the performance of FQPSK when the detector makes decisions on a symbol-by-symbol basis, i.e., the inherent memory introduced by the trellis coding is ignored at the receiver. In order to understand how this can be accomplished, we first will establish the fact that, in any typical transmission interval, there exists a fixed number (in particular, eight) of possible waveforms (pulse shapes) that represent the FQPSK signal and each of these occurs with equal probability. As such, from symbol to symbol, the FQPSK signal appears as an equiprobable M-ary signaling set (with $M = 8$) and thus can be detected accordingly. With this in mind, we shall investigate two possible simple structures, both of which are suboptimum relative to the trellis-coded receiver previously discussed, that exploit the memory inherent in the modulation. The first structure is a standard offset QPSK receiver that employs simple integrate and dumps (I&Ds) as detectors and as such ignores the pulse shaping associated with the above-mentioned M-ary symbol-by-symbol representation. The second structure, which shall be referred to as an average matched-filter receiver, improves on the first one by replacing the I&Ds with matched filters, where the match is made to the *average* of the waveshapes in the M-ary signal set representation. Without loss in generality, the following description shall consider the case $n = 0$ corresponding to the I-channel interval $-T_s/2 \le t \le T_s/2$ and the Q-channel interval $0 \le t \le T_s$. We shall focus our attention on only the I channel and, as such, our initial goal will be to determine the eight equally likely waveforms that typify an FQPSK waveform in the interval $0 \le t \le T_s$. To avoid confusion with the previously defined signals, such as those defined, for example, in Eqs. (7a) and (7b), we shall use upper case notation, i.e., $S_i(t)$, $i = 0, 1, \cdots, 7$ to describe these new waveforms. As we shall see, each of these new waveforms shall be composed of the latter half (i.e., that which occurs in the interval $0 \le t \le T_s/2$) of the I-channel waveform transmitted in the interval $-T_s/2 \le t \le T_s/2$ followed by the first half (i.e., that which occurs in the interval $T_s/2 \le t \le T_s$) of the I-channel waveform transmitted in the interval $T_s/2 \le t \le 3T_s/2$. As stated above, it will be shown that only eight such possible combinations can exist, and all are equiprobable.

A. Signal Representation

Let $d_{I0} = 1$, or equivalently from Eq. (10), $D_{I0} = 0$. Then, from Table 1, corresponding to $d_{I,-1} = 1$ (which results in $|(d_{I0} - d_{I,-1})/2| = 0$), there are four possible waveforms, $(s_0(t), s_1(t), s_2(t),$ and $s_3(t))$ that can be transmitted. Likewise corresponding to $d_{I,-1} = -1$ (which results in $|(d_{I0} - d_{I,-1})/2| = 1$), there are four possible waveforms, $(s_4(t), s_5(t), s_6(t),$ and $s_7(t))$, that can be transmitted. In each case, which of the four possible waveforms is transmitted depends on the difference values associated with $d_{Q,-2}, d_{Q,-1}$, and d_{Q0} in accordance with the second and third columns of Table 1. While, in principle, for each possible waveform $s_i(t)$ transmitted in $-T_s/2 \le t \le T_s/2$ there are eight possible waveforms that can be transmitted in $T_s/2 \le t \le 3T_s/2$, it is straightforward to show that only four

[7] Needless to say, at smaller (finite) signal-to-noise ratios (SNRs), the loss between uncoded OQPSK and trellis-decoded FQPSK will be even less.

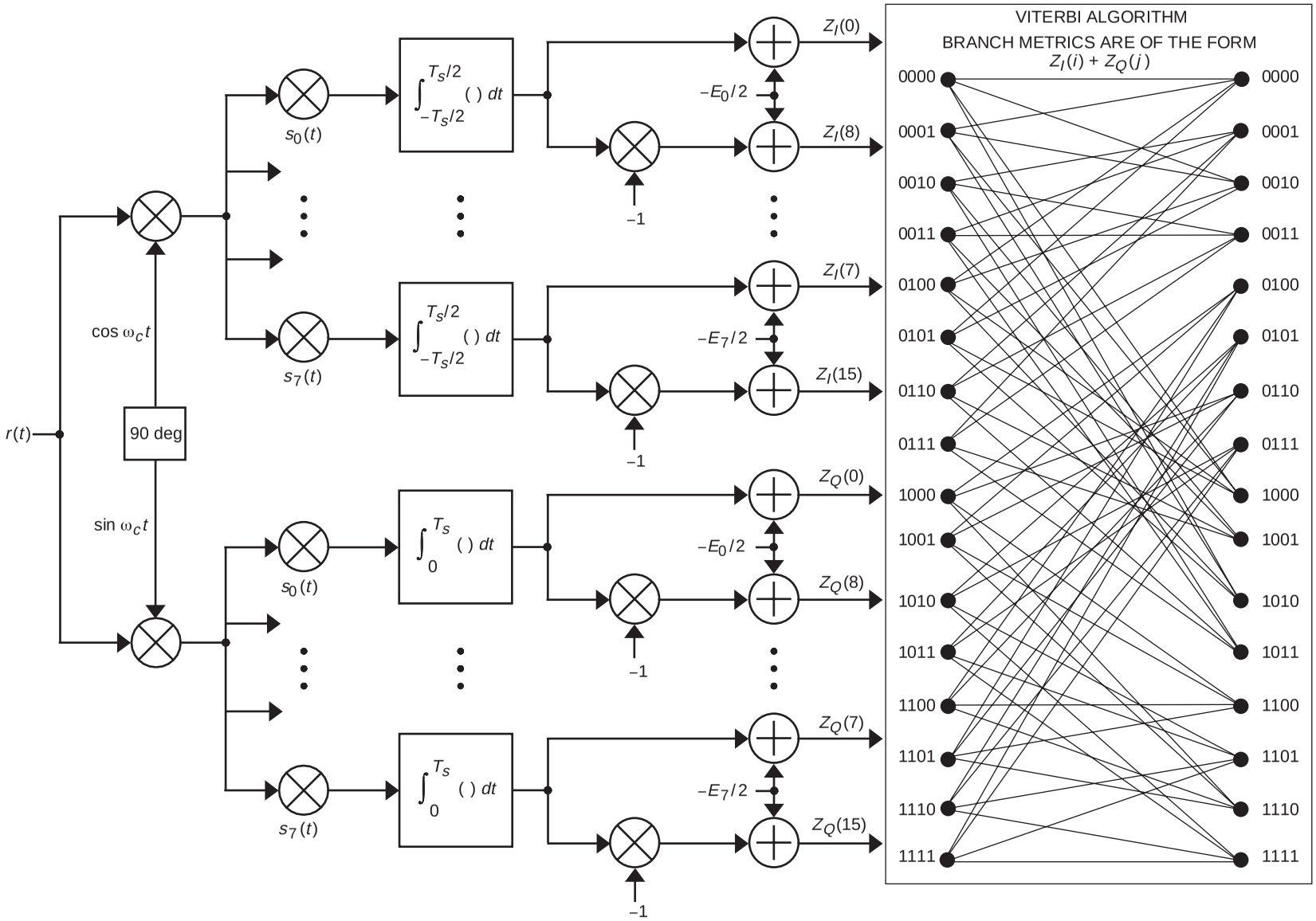

Fig. 11. The optimum trellis-coded receiver for FQPSK.

of these eight are unique. For example, if $s_0(t)$ is transmitted in $-T_s/2 \le t \le T_s/2$ (corresponding, as above, to $d_{I,-1} = 1$), then the four possible waveforms that can occur in $T_s/2 \le t \le 3T_s/2$ are $s_0(t), s_1(t), s_{12}(t)$, and $s_{13}(t)$. Thus, corresponding to the I-channel signal $s_I(t) = s_0(t)$ in the interval $-T_s/2 \le t \le T_s/2$, the transmitted signal $S_i(t)$ for the interval $0 \le t \le T_s$ is composed of the latter half of $s_0(t)$ followed by the first half of either $s_0(t), s_1(t), s_{12}(t)$, or $s_{13}(t)$. Looking at the definitions of $s_0(t), s_1(t), s_{12}(t)$, and $s_{13}(t)$ in Eqs. (7a) and (7b), we see that this yields only two distinct possibilities for $S_i(t)$, namely,

$$\left.\begin{aligned} S_0(t) &= A, \quad 0 \le t \le T_s \\ S_1(t) &= \begin{cases} A, & 0 \le t \le \dfrac{T_s}{2} \\ \sin\dfrac{\pi t}{2T_s}, & \dfrac{T_s}{2} \le t \le T_s \end{cases} \end{aligned}\right\} \tag{22a}$$

both of which are equally likely. Thus, in summary, for $d_{I0} = 1$ and $s_I(t) = s_0(t)$ in the interval $-T_s/2 \le t \le T_s/2$, there are only two waveforms that can occur in $0 \le t \le T_s$, namely, $S_0(t)$ and $S_1(t)$ of Eq. (22a).

Following a similar procedure (still for $d_{I0} = 1$), it can be shown that, for each of the other possible waveforms in $-T_s/2 \le t \le T_s/2$, i.e., $s_1(t), s_2(t), s_3(t), s_4(t), s_5(t), s_6(t)$, and $s_7(t)$, there are four waveforms that can occur in the succeeding interval $T_s/2 \le t \le 3T_s/2$ but only two possible distinct waveforms in $0 \le t \le T_s$. These possibilities are summarized in Table 4.

The signals $S_2(t), S_3(t), S_4(t), S_5(t), S_6(t)$, and $S_7(t)$ are defined as

$$\left.\begin{aligned} S_2(t) &= 1 - (1-A)\cos^2\frac{\pi t}{T_s}, \quad 0 \le t \le T_s \\ S_3(t) &= \begin{cases} 1-(1-A)\cos^2\dfrac{\pi t}{T_s}, & 0 \le t \le \dfrac{T_s}{2} \\ \sin\dfrac{\pi t}{2T_s}, & \dfrac{T_s}{2} \le t \le T_s \end{cases} \\ S_4(t) &= \begin{cases} A\sin\dfrac{\pi t}{2T_s}, & 0 \le t \le \dfrac{T_s}{2} \\ A, & \dfrac{T_s}{2} \le t \le T_s \end{cases} \\ S_5(t) &= A\sin\frac{\pi t}{2T_s}, \quad 0 \le t \le T_s \\ S_6(t) &= \begin{cases} \sin\dfrac{\pi t}{2T_s}, & 0 \le t \le \dfrac{T_s}{2} \\ 1-(1-A)\cos^2\dfrac{\pi t}{T_s}, & \dfrac{T_s}{2} \le t \le T_s \end{cases} \\ S_7(t) &= \sin\frac{\pi t}{2T_s}, \quad 0 \le t \le T_s \end{aligned}\right\} \tag{22b}$$

Table 4. Possible $S_i(t)$'s for successive combinations of $s_i(t)$.

Signal in $-T_s/2 \le t \le T_s/2$	Signal in $T_s/2 \le t \le 3T_s/2$	Signal in $0 \le t \le T_s$
$s_1(t)$	$s_2(t), s_3(t), s_{14}(t), s_{15}(t)$	$S_2(t), S_3(t)$
$s_2(t)$	$s_0(t), s_1(t), s_{12}(t), s_{13}(t)$	$S_0(t), S_1(t)$
$s_3(t)$	$s_2(t), s_3(t), s_{14}(t), s_{15}(t)$	$S_2(t), S_3(t)$
$s_4(t)$	$s_0(t), s_1(t), s_{12}(t), s_{13}(t)$	$S_4(t), S_5(t)$
$s_5(t)$	$s_2(t), s_3(t), s_{14}(t), s_{15}(t)$	$S_6(t), S_7(t)$
$s_6(t)$	$s_0(t), s_1(t), s_{12}(t), s_{13}(t)$	$S_4(t), S_5(t)$
$s_7(t)$	$s_2(t), s_3(t), s_{14}(t), s_{15}(t)$	$S_6(t), S_7(t)$

In comparing the performances of the suboptimum receivers of FQPSK with that of uncoded OQPSK, we shall reference them all to the same average transmitted power, $\bar{P}$, or, equivalently, the same average energy-per-bit-to-noise spectral density ratio, $\bar{E}_b/N_0 = \bar{P}T_b/N_0$. In order to do this, we first must compute the energy $E_i = \int_0^{T_s} S_i^2(t)\,dt$ of each of the waveforms in Eqs. (22a) and (22b) and take their average. The results are summarized below:

$$\left.\begin{aligned}
E_0 &= A^2 T_s \\
E_1 &= \frac{3}{4}A^2 T_s \\
E_2 &= \left(\frac{3}{8} + \frac{1}{4}A + \frac{3}{8}A^2\right) T_s \\
E_3 &= \left(\frac{7}{16} + \frac{1}{8}A + \frac{3}{16}A^2\right) T_s \\
E_4 &= \frac{3}{4}A^2 T_s \\
E_5 &= \frac{1}{2}A^2 T_s \\
E_6 &= \left(\frac{7}{16} + \frac{1}{8}A + \frac{3}{16}A^2\right) T_s \\
E_7 &= \frac{1}{2}T_s
\end{aligned}\right\} \tag{23}$$

and

$$\bar{E} = \frac{1}{8}\sum_{i=0}^{7} E_i = \left(\frac{7 + 2A + 15A^2}{32}\right) T_s \tag{24}$$

Since the average power transmitted in the I channel is one-half the total $(I+Q)$ average transmitted power, $\bar{P}$, then we have

$$\frac{\bar{P}}{2} = \frac{\bar{E}}{T_s} = \frac{7+2A+15A^2}{32} \tag{25}$$

or, equivalently, the average energy per symbol is given by

$$\bar{P}T_s \triangleq \bar{E}_s = 2\bar{E}_b = \frac{7+2A+15A^2}{16}T_s \tag{26}$$

Comparing Eq. (26) with Eq. (16), we see that the evaluation of average energy per symbol based on the symbol-by-symbol M-ary representation of FQPSK is identical to that obtained from the representation as a trellis-coded modulation. Also note that for $A=1$, which corresponds to SQORC modulation, we have $\bar{E}_s = (4/3)T_s$, which is consistent with the original discussions of this modulation in [7].

B. Suboptimum Receivers

In accordance with our discussion at the beginning of Section VI, we shall consider two suboptimum receivers for symbol-by-symbol detection of FQPSK, the difference being the manner in which the detector is matched to the received signal. For the average matched-filter case, the detector is implemented as a multiplication of the received signal by $\bar{S}(t) \triangleq (1/8)\sum_{i=0}^{7} S_i(t)$, followed by an I&D filter and binary hard-decision device (see Fig. 11). For the OQPSK receiver, the detector is purely I&D (i.e., matched to a rectangular pulse), which is tantamount to assuming $\bar{S}(t) = 1$. Thus, we can cover both cases at the same time, leaving $\bar{S}(t)$ as an arbitrary premultiplication pulse shape, and later substitute the appropriate waveform.

Assuming the M-ary symbol-by-symbol representation of FQPSK just described, then the decision variable Z in Fig. 12 is given by

$$Z = \int_0^{T_s} S(t)\,\bar{S}(t)\,dt + \int_0^{T_s} n(t)\,\bar{S}(t)\,dt \triangleq \bar{Z} + N \tag{27}$$

where $S(t)$ is the transmitted waveform in $0 \le t \le T_s$ and ranges over the set of eight waveforms in Eqs. (22a) and (22b) with equal probability. The random variable N is zero-mean Gaussian with variance $\sigma_N^2 = N_0 E_{\bar{S}}/2$, where $E_{\bar{S}} \triangleq \int_0^{T_s} \bar{S}^2(t)\,dt$. Thus, the I-channel symbol-error probability (same as the Q-channel symbol-error probability) conditioned on the particular $S(t) = S_i(t)$ corresponding to the transmitted symbol $d_{I0} = 1$ is easily shown to be

$$P_{si}(E) = \frac{1}{2}\,\mathrm{erfc}\left(\sqrt{\frac{1}{N_0}\frac{\left(\int_0^{T_s} S_i(t)\,\bar{S}(t)\,dt\right)^2}{E_{\bar{S}}}}\right) \tag{28}$$

and, hence, the average symbol-error probability is given by

$$P_s(E) \triangleq \frac{1}{8}\sum_{i=0}^{7} P_{si}(E) \tag{29}$$

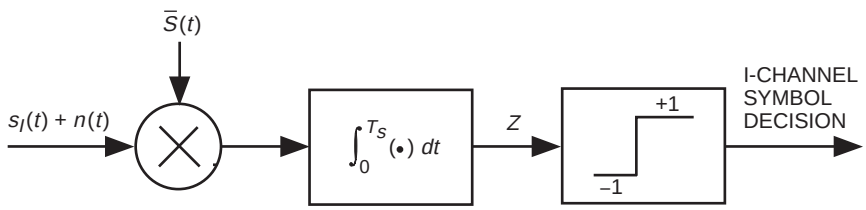

Fig. 12. The suboptimum receiver for FQPSK based on symbol-by-symbol detection.

1. Conventional OQPSK Receiver. For the conventional OQPSK receiver, we set $\bar{S}(t) = 1$, or, equivalently, $E_{\bar{S}} = T_s$ in Eq. (28), resulting in

$$P_{si}(E) = \frac{1}{2}\,\mathrm{erfc}\left(\sqrt{\frac{T_s}{N_0}\left(\frac{1}{T_s}\int_0^{T_s} S_i(t)\,dt\right)^2}\right) = \frac{1}{2}\,\mathrm{erfc}\left(\sqrt{\left(\frac{32}{7+2A+15A^2}\right)\frac{\bar{E}_b}{N_0}\left(\frac{E_i}{T_s}\right)^2}\right) \tag{30}$$

Substituting the average energies from Eq. (23) in Eq. (30) for each signal and then performing the average as in Eq. (29) gives the final desired result for average symbol-error probability, namely,

$$\begin{aligned} P_{si}(E) = {} & \frac{1}{16}\,\mathrm{erfc}\left(\sqrt{\left(\frac{32A^4}{7+2A+15A^2}\right)\frac{\bar{E}_b}{N_0}}\right) + \frac{1}{8}\,\mathrm{erfc}\left(\sqrt{\left(\frac{18A^4}{7+2A+15A^2}\right)\frac{\bar{E}_b}{N_0}}\right) \\ & + \frac{1}{16}\,\mathrm{erfc}\left(\sqrt{\left(\frac{(3+2A+3A^2)^2}{2(7+2A+15A^2)}\right)\frac{\bar{E}_b}{N_0}}\right) + \frac{1}{8}\,\mathrm{erfc}\left(\sqrt{\left(\frac{(7+2A+3A^2)^2}{8(7+2A+15A^2)}\right)\frac{\bar{E}_b}{N_0}}\right) \\ & + \frac{1}{16}\,\mathrm{erfc}\left(\sqrt{\left(\frac{8A^4}{7+2A+15A^2}\right)\frac{\bar{E}_b}{N_0}}\right) + \frac{1}{16}\,\mathrm{erfc}\left(\sqrt{\left(\frac{8}{7+2A+15A^2}\right)\frac{\bar{E}_b}{N_0}}\right) \end{aligned} \tag{31}$$

2. Average Matched-Filter Receiver. For the average matched filter, we need to compute the correlations of each of the pulse shapes in Eqs. (22a) and (22b) with the average pulse shape $\bar{S}(t)$ and also the energy $E_{\bar{S}}$ of the average pulse shape. Rewriting Eq. (28) in a form analogous to Eq. (30), namely,

$$P_{si}(E) = \frac{1}{2}\,\mathrm{erfc}\left(\sqrt{\left(\frac{32}{7+2A+15A^2}\right)\frac{\bar{E}_b}{N_0}\,\frac{\left(\frac{1}{T_s}\int_0^{T_s} S_i(t)\,\bar{S}(t)\,dt\right)^2}{\frac{1}{T_s}E_{\bar{S}}}}\right) \tag{32}$$

then the results necessary to evaluate Eq. (32) are tabulated below:

$$
\left.
\begin{aligned}
&\frac{1}{T_s}\int_0^{T_s} S_0(t)\,\bar{S}(t)\,dt = \frac{A}{4}\left[\frac{1}{2}+\frac{2}{\pi}+A\left(\frac{3}{2}+\frac{2}{\pi}\right)\right] \\
&\frac{1}{T_s}\int_0^{T_s} S_1(t)\,\bar{S}(t)\,dt = \frac{1}{T_s}\int_0^{T_s} S_4(t)\,\bar{S}(t)\,dt = \frac{A}{4}\left[\frac{1}{2}+\frac{5}{3\pi}+A\left(1+\frac{7}{3\pi}\right)\right] \\
&\frac{1}{T_s}\int_0^{T_s} S_2(t)\,\bar{S}(t)\,dt = \frac{1}{4}\left[\frac{3}{8}+\frac{4}{3\pi}+A\left(\frac{3}{4}+\frac{2}{\pi}\right)+A^2\left(\frac{7}{8}+\frac{2}{3\pi}\right)\right] \\
&\frac{1}{T_s}\int_0^{T_s} S_3(t)\,\bar{S}(t)\,dt = \frac{1}{T_s}\int_0^{T_s} S_6(t)\,\bar{S}(t)\,dt = \frac{1}{4}\left[\frac{7}{16}+\frac{4}{3\pi}+A\left(\frac{5}{8}+\frac{7}{3\pi}\right)+A^2\left(\frac{7}{16}+\frac{1}{3\pi}\right)\right] \\
&\frac{1}{T_s}\int_0^{T_s} S_5(t)\,\bar{S}(t)\,dt = \frac{A}{2}\left[\frac{1}{4}+\frac{2}{3\pi}+A\left(\frac{1}{4}+\frac{4}{3\pi}\right)\right] \\
&\frac{1}{T_s}\int_0^{T_s} S_7(t)\,\bar{S}(t)\,dt = \frac{1}{2}\left[\frac{1}{4}+\frac{2}{3\pi}+A\left(\frac{1}{4}+\frac{4}{3\pi}\right)\right]
\end{aligned}
\right\} \tag{33}
$$

and

$$
\frac{1}{T_s}E_{\bar{S}} = \frac{1}{16}\left[(1+A)^2\left(\frac{3}{2}+\frac{4}{\pi}\right)+\frac{3}{8}(1-A)^2-2\left(1-A^2\right)\left(\frac{1}{2}+\frac{2}{3\pi}\right)\right] \tag{34}
$$

Finally, substituting Eqs. (33) and (34) into Eq. (32) and averaging as in Eq. (29) gives the desired result, which we shall not explicitly write in closed form.

VII. Average Bit-Error Probability Performance

The average BEP of the two suboptimum receivers discussed in Section VI is illustrated in Fig. 13 for the case $A = 1/\sqrt{2}$, which is the usual value chosen for implementation of FQPSK. These results are obtained directly from Eq. (31) for the OQPSK receiver and from Eq. (29) in combination with Eqs. (32) through (34) for the average matched-filter receiver. Also included in this figure is the performance corresponding to the optimum uncoded OQPSK receiver (same performance as for uncoded BPSK), i.e., $P_b(E) = 1/2\ \mathrm{erfc}\sqrt{E_b/N_0}$, as well as simulation results obtained for the optimum trellis-coded receiver of Fig. 11. We observe, as one might expect, that the average matched-filter receiver outperforms the OQPSK receiver, since an attempt to match the transmitted pulse shape (even on an average basis) is better than no attempt at all. We also observe that the trellis-coded receiver at $P_b(E) = 10^{-4}$ is more than 1-dB better than the average matched-filter receiver, granted that the latter is considerably simpler in implementation. Finally, for the same average BEP, the trellis-coded receiver of FQPSK is only about 0.6-dB inferior to uncoded OQPSK performance, which is a relatively small penalty paid for the vast improvement in PSD afforded by the former relative to the latter.

VIII. Conclusion

By offering a new interpretation of unfiltered FQPSK in terms of a full (as opposed to a half) symbol mapping of an I and Q error-correction coded modulation, we have been able to provide methods for enhancing its spectral properties as well as its error-probability performance. Similar methods can be applied to filtered versions of FQPSK.

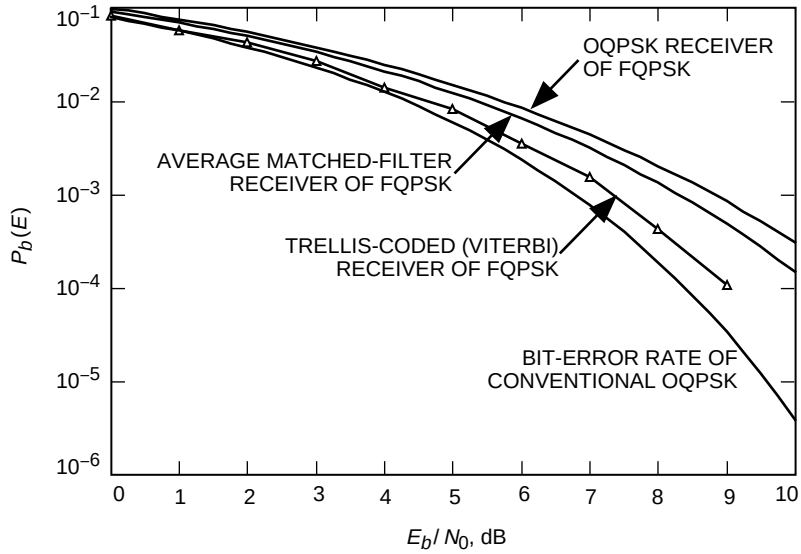

Fig. 13. Bit-error performance of various receivers of FQPSK modulation (the reference curve is the bit-error rate of OQPSK).

Acknowledgment

The authors wish to gratefully acknowledge Meera Srinivasan for simulating the optimum trellis-coded receiver of FQPSK (Fig. 11) and supplying the accompanying numerical results shown in Fig. 13. Additional thanks also are due to Meera for having spent considerable time independently verifying much of what is presented here, which is immeasurably important in establishing the credence of our results.

References

[1] K. Feher and S. Kato, U.S. Patent 4,567,602; K. Feher, U.S. Patent 5,491,457; and K. Feher, U.S. Patent 5,784,402.

[2] K. Feher, *Wireless Digital Communications: Modulation and Spread Spectrum Applications*, Englewood Cliffs, New Jersey: Prentice-Hall, 1995.

[3] K. Feher, "FQPSK Doubles Spectral Efficiency of Operational Telemetry Systems," European Telemetry Conference, ETC '98, Garmish-Patternk, Germany, May 5–8, 1998.

[4] S. Kato and K. Feher, "XPSK: A New Cross-Correlated Phase-Shift-Keying Modulation Technique," *IEEE Transactions on Communications*, vol. 31, no. 5, pp. 701–707, May 1983.

[5] W. L. Martin, T-Y. Yan, and L. V. Lam, "CCSDS-SFCG: Efficient Modulation Methods Study at NASA/JPL, Phase 3: End-to-End Performance," SFCG Meeting, Galveston, Texas, September 1997.

[6] T. Le-Ngoc, K. Feher, and H. Pham Van, "New Modulation Techniques for Low-Cost Power and Bandwidth Efficient Satellite Earth Stations," *IEEE Transactions on Communications*, vol. 30, no. 1, pp. 275–283, January 1982.

[7] M. C. Austin and M. V. Chang, "Quadrature Overlapped Raised-Cosine Modulation," *IEEE Transactions on Communications*, vol. 29, no. 3, pp. 237–249, March 1981.

[8] J. B. Anderson, T. Aulin, and C.-E. Sundberg, *Digital Phase Modulation*, New York: Plenum Press, p. 29, 1986.